Impulse absorption by tapered horizontal alignments of elastic spheres

Robert L. Doney*
U.S. Army Research Laboratory, Aberdeen Proving Grounds, Maryland 21005, USA
and Department of Physics, State University of New York at Buffalo, Buffalo, New York 14260-1500, USA

Surajit Sen†
Department of Physics, State University of New York at Buffalo, Buffalo, New York 14260-1500, USA
(Received 26 June 2005; published 19 October 2005)

We present an analytical and numerical study of the problem of mechanical impulse propagation through a horizontal alignment of progressively shrinking (tapered) elastic spheres that are placed between two rigid end walls. The studies are confined to cases where initial loading between the spheres is zero (i.e., in the "sonic vacuum" region). The spheres are assumed to interact via the Hertz potential. Force and energy as a function of time for selected grains that comprise the solitary wave are provided and shed light on the system's behavior. Propagation of energy is analytically studied in the hard-sphere approximation and phase diagrams plotting normalized kinetic energy of the smallest grain at the tapered end are developed for various chain lengths and tapering factors. These details are then compared to kinetic energy phase diagrams obtained via extensive dynamical simulations. Our figures indicate that the ratios of the kinetic energies of the smallest to largest grains possess a Gaussian dependence on tapering and an exponential decay when the number of grains increases. The conclusions are independent of system size, thus being applicable to tapered alignments of micron-sized spheres as well as those that are macroscopic and more easily realizable in the laboratory. Results demonstrate the capabililty of these chains to thermalize propagating impulses and thereby act as potential shock absorbing devices.

DOI: 10.1103/PhysRevE.72.041304 PACS number(s): 83.80.Fg, 05.45.−a, 62.50.+p

I. INTRODUCTION

It is always desirable to look for new technologies which may provide breakthroughs, or, at the minimum, increase the capability to perform some critical task by an appropriate amount. Shock mitigation is one such area that will always be receptive to improvements in the state of the art. For one thing, it encapsulates several important applications of military and public interest such as blast-proofing and vibrational dampening. These two categories alone can create a long list of specific applications.

One area that holds potential and is being investigated heavily is granular systems [1–6]. While granular media has been used for shock absorption for decades against ballistics (sandbags), new features are being observed in the growing literature which suggest that a more technological role may be at hand. Particularly appealing and relatively simple to address is the behavior of one-dimensional (1D) systems where smooth elastic spheres that are barely touching are placed adjacent to each other in a horizontal alignment. Even though we may constrain the basis of this system to just a few parameters, the complexity of its dynamics is formidable [7–15]. One such family of systems is the tapered chain (TC) [16,17].

The TC (Fig. 1) is a granular alignment of elastic spheres that touch at a single point in their initial state. When the grains are under compression, the contact regions grow from being points to disks along the plane orthogonal to that of Fig. 1. It can be characterized by the number of grains N, the successive decrease in the radius of the grains or "tapering" q, and restitutive losses ω. Adjacent grains interact through a potential developed by Hertz [18] and discussed in several readily accessible publications [19–21]. We note that Nesterenko [22] has written extensively on the dynamics of granular chains.

The Hertz potential can be written as

$$V(\delta_{i,i+1}) = \frac{2}{5D}\sqrt{\frac{R_i R_{i+1}}{R_i + R_{i+1}}}\,\delta_{i,i+1}^{5/2} \equiv a_{i,i+1}\delta_{i,i+1}^{5/2}, \qquad (1)$$

where

$$D = \frac{3}{4}\left(\frac{1-\sigma_i^2}{E_i} + \frac{1-\sigma_{i+1}^2}{E_{i+1}}\right). \qquad (2)$$

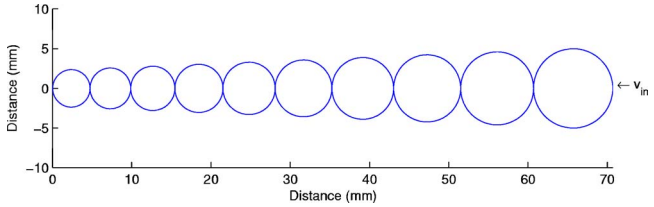

FIG. 1. (Color online) A tapered chain is shown with number of grains $N=10$, tapering $q=8\%$, length $L=70.7$ mm, and radius of the largest grain as 5 mm. In our simulations, an initial velocity is applied to the largest sphere.

*Electronic address: bdoney@arl.army.mil
†Electronic address: sen@dynamics.physics.buffalo.edu

Here, $\delta_{i,i+1}=R_i+R_{i+1}-(z_{i+1}-z_i)>0$, represents the overlap between successive grains where z_j is their position. Additionally, $a_{i,i+1}$ has been defined for material properties: E_j is the Young's modulus and σ_j is the Poisson ratio and radii R_j. Note that j can refer to either particle i or $i+1$.

If $\delta_{i,i+1}\leqslant 0$ then $V=0$ since adjacent grains i and $i+1$ have lost contact. It may be noted that Eq. (1) describes a repulsive potential that grows faster than a quadratic form of $\delta_{i,i+1}$. The Hertz repulsion is hence a nonlinear force. More specifically, the repulsion is softer than something harmonic over short distances, but becomes steeper than a harmonic form with increasing compression. An extreme case would be the hard-sphere potential. We shall discuss the dynamics of the TC both in terms of the Hertz and hard-sphere potentials and address the shortcomings of a hard-sphere treatment in granular dynamics problems. For our particular study, all materials are the same in any *single* tapered chain so that Eq. (2) reduces to

$$D=\frac{3}{2}\left(\frac{1-\sigma^2}{E}\right). \tag{3}$$

In this work we focus on the dynamics of the TC. What distinguishes this study from earlier research [14] is the focus on tapered rather than monodisperse ($q=0$) chains. As discussed elsewhere [7–15,17], any impulse propagates as a solitary wave through these chains. Such solitary wave propagation studies are closely linked to research on nonlinear lattices [23–31]. Here we are interested in evaluating the effects of tapering on granular alignments. The traveling pulse must break down to smaller energy bundles at every interface. Additionally, we asked the questions: how does the motion of grains at the end of chains differ as a function of tapering? What do the parameter spaces look like for such a large variety of configurations? And how do these compare with a simple hard-sphere approximation treatment of the dynamics of a TC? If one can show significant reduction in output energy while ensuring that the structure of granular alignments can be maintained, it is quite possible to use these TCs against propagating shocks. For now, we assume that the input energy is such that one remains within the elastic regime.

We present the study as follows. In Sec. II we discuss the numerical solution to the equations of motion of the TC. We present extensive dynamical analyses summarized via appropriate "phase diagrams" to illustrate the shock absorbing properties of TCs. From the dynamical behavior of the first and the last particles, the normalized energy and force can be plotted as functions of the parametric variables; for example, the kinetic energy T is studied as functions of the number of grains in the system and the tapering. We further probe the system dynamics by adjusting restitutive losses—defined herein as an imbalance between the forces of compression and unloading of the spheres. In Sec. III, a hard-sphere approximation is pursued to study the propagation of an impulse incident on the largest sphere of a TC such that compressive effects are ignored. A functional fit is then developed in Sec. IV which estimates $T(\omega,q)$ for $N=20$. We conclude in Sec. V with a summary and description of continuing work.

II. DYNAMICAL STUDIES

The equation of motion for grain m_i at position z_i is constructed from the potential in Eq. (1). In the case where the grains are not precompressed, the equation of motion is

$$m_i\ddot{z}_i=\frac{5}{2}(a_{i-1,i}\delta_{i-1,i}^{3/2}-a_{i,i+1}\delta_{i,i+1}^{3/2}). \tag{4}$$

It is important to note that the right-hand side of Eq. (4) involves purely nonlinear terms, i.e., a perturbation about linear forces is not possible in our problem. As discussed extensively by Nesterenko and others [7–16], the TC systems belong to the category of nonlinear systems where sound propagation is prohibited, the so-called "sonic vacua" systems.

In our analyses, restitutional loss [33,34] has been defined as follows:

$$\frac{F_{unloading}}{F_{loading}}=1-\omega, \tag{5}$$

where $F_{loading}$ represents the loading force between two adjacent grains as they press against each other and $F_{unloading}$ is the unloading force between the grains as they come apart. If $F_{loading}>F_{unloading}$, energy is lost in the work done by the forces during loading and subsequent unloading. The restitution coefficient ω defined above is not well known for most materials. We hence treat ω as a free parameter and explore system dynamics for reasonable values of ω. As per our definition of ω, perfectly elastic collisions correspond to $\omega=0$.

We report our results from extensive dynamical simulations of impulse propagation through TCs for different values of N, q, and ω. We have chosen to use SiC [35], a well-studied, hard material, as that which makes up the grains when $\omega\neq 0$. The shock absorption properties of the system are influenced by N, q, and ω only as is evident from the simple analyses that led to the derivation of Eq. (4). For SiC, we use density $\rho=3.2\ \mathrm{mg/mm^3}$ and $D=0.003\,266\ \mathrm{mm^2/kN}$. The dynamical simulations were performed using a velocity Verlet algorithm [36] for $3\leqslant N\leqslant 20$ and $0\leqslant q,\omega\leqslant 0.1$ over a system time of 1 ms where the time step was set to 10 ps with 10^8 steps in the integration loop. It should be noted that the fundamental unit of force in our simulations is the kilonewton. In addition, for each chain, an initial velocity of 0.01 mm/μs (10 m/s) is applied to the largest end.

A. Time-dependent behavior of grains

In this section, we examine the dynamics of the smallest grain in the TC to get an idea of how kinetic energy is transported from the largest grain to the smallest grain in the system, to see how the walls affect energy transport and to examine the role of restitution in attenuating the propagating kinetic energy. It should be noted that in the Hertz system [18], a significant part of the impulse ends up being stored as potential energy in the intergranular contacts at different times [37].

Figures 2 and 3 reveal the temporal behavior of the smallest grain for several q values (including the important case of

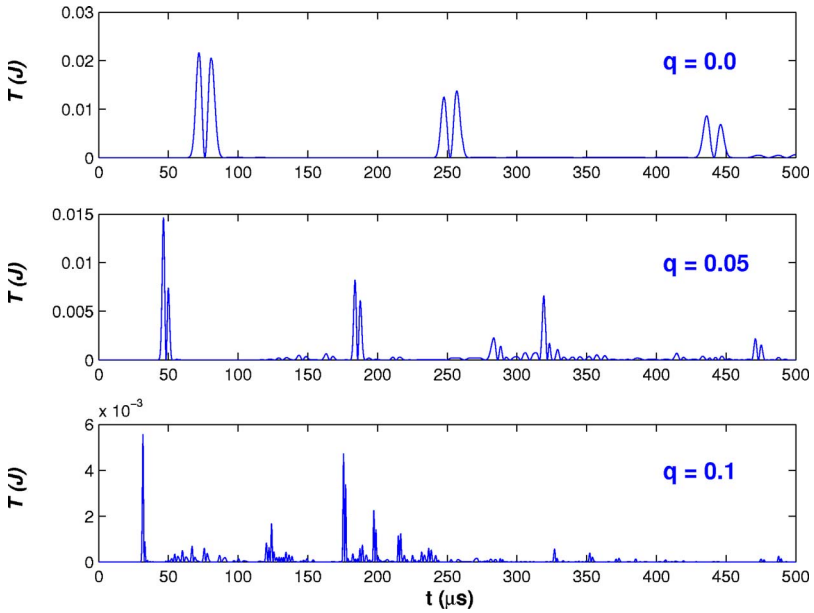

FIG. 2. (Color online) Kinetic energy as a function of time for the last grain (left-most grain in Fig. 1, for example) in a chain with $N=15, \omega=0.05$. Each plot is evaluated for a different tapering with initial T as 0.0838 J. Note that as one strengthens the tapering q for otherwise identical chains, well-defined pulses are increasingly converted into noise.

$q=0$, i.e., the monodisperse chain, where solitary wave propagation is encountered [7–16]) in a TC where $\omega=0.05$ and $N=15$, 20, respectively. For clarity, these plots only represent the first half of the total simulation time. The double-peak structure of the T maxima relate to the fact that the last grain, meaning the grain that is farthest from the impulse initiation point, hits the wall, stops, and then rebounds. Note the decreasing scale of T in each underlying panel in both figures. The T scales as v^2 and m^1 thus one might expect it to increase with larger tapering due to the higher velocities. However, $m \propto r^3 \sim (1-q)^3$ and this dominates. Width of the peaks, which is related to particle velocities, are functions of q and N. As q increases, the initial peaks are shifted to earlier times and signal transmission is therefore faster. Higher velocities also imply more collisions and therefore more restitutive losses. Note that in both cases, a single, well-defined pulse has been turned into "less audible" noise by increasing the tapering in the system. Comparison of the data between Figs. 2 and 3 reveals that changing N from 15 to 20 leads to a significant change in the shock absorption properties of the TC. Note also the large peak in Fig. 3 for $q=0.1$. This is an unexpected result and is discussed in more detail in the Appendix with regard to normalizing the kinetic energy. To better understand the dynamics, we can address the behavior of several adjoining grains near the boundary.

Figure 4 contrasts the displacements from equilibrium, velocities, and kinetic energies for the last five grains (particles 11–15) between a monodisperse [panels (a)–(c)] and a tapered [panels (d)–(f)] chain. In particular, let us examine two chains in Fig. 2 represented by the top panel (monodisperse) and the bottom panel (10% tapering). Particle 15 is the last grain and is in contact with the boundary. The subplots on the left [panels (a)–(c)] of Fig. 4 represent the monodisperse chain where each grain has $r=5$ mm. The right half

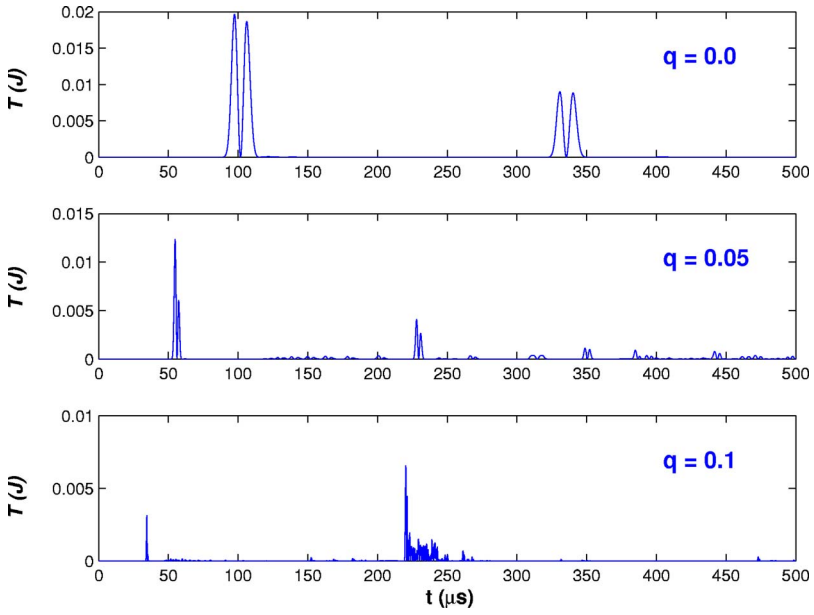

FIG. 3. (Color online) Kinetic energy as a function of time for the last grain in a chain with $N=20, \omega=0.05$. Each plot is evaluated for a different tapering with initial T as 0.0838 J. The overall effect is congruent to Fig. 2: an impulse is greatly spread out over time. Additionally, amplitudes are diminished due to the increase in N.

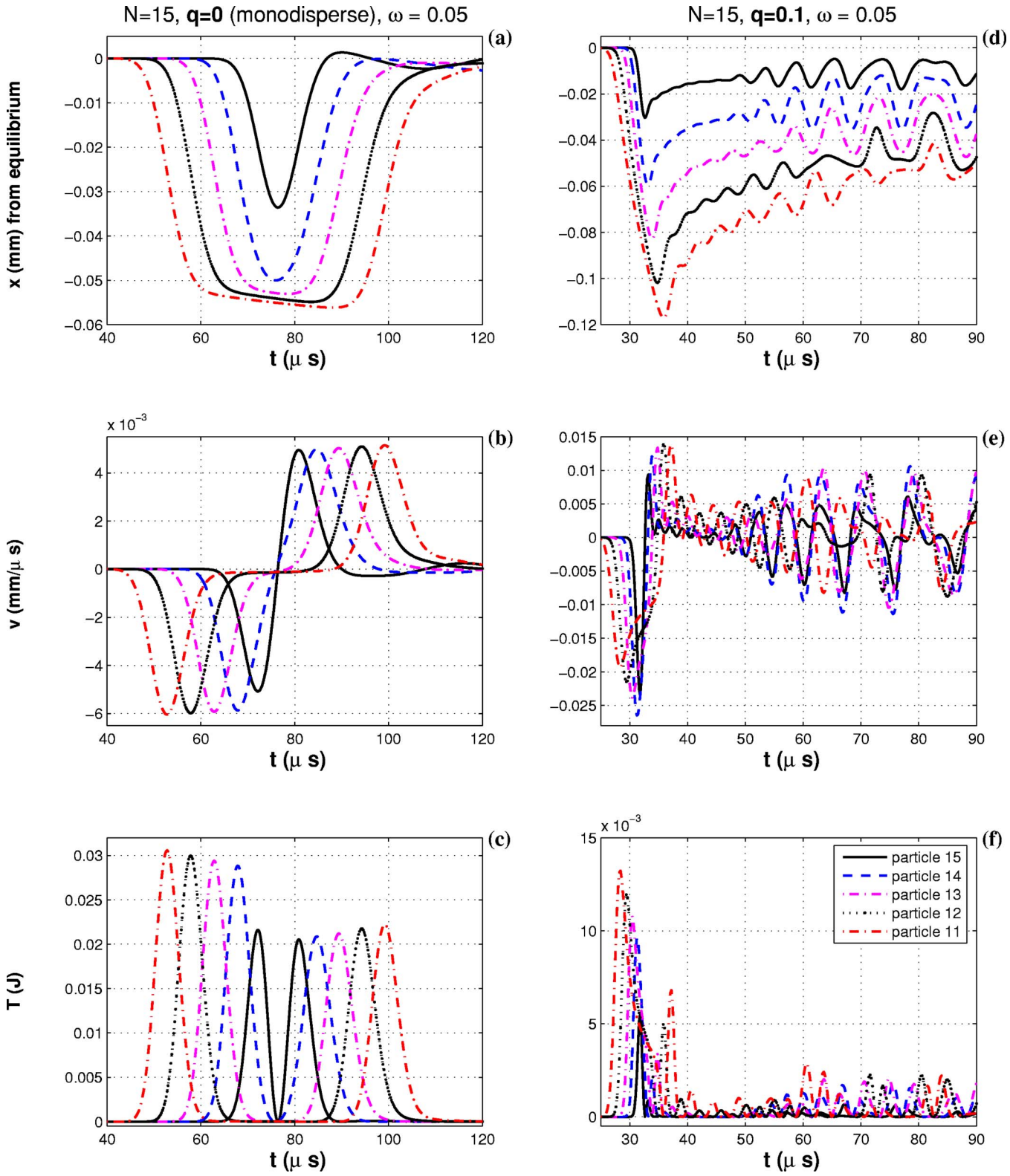

FIG. 4. (Color online) Absolute positions, velocities, and kinetic energies for particles 11–15. Particle 15 is the last grain and is in contact with the boundary. The subplots (a)–(c) represent the monodisperse chain where each grain has $r=5$ mm and an impulse propagates as a solitary wave, while (d)–(f) correspond to a chain with a tapering of 10% so that particles 11–15 have radii 1.74, 1.57, 1.41, 1.27, and 1.14 mm, respectively. These subplots illustrate when the grains in question first receive the incident impulse. Note the earlier time of arrival for $q=0.1$ since velocities are higher (up to a factor of 4 in the plots). For panels (d)–(f) the dynamics have been extended beyond initial incidence and reflection. Also visible in panel (f) is how the impulse is spread out over time and space (grains) as opposed to the clear signal transmission in panel (c).

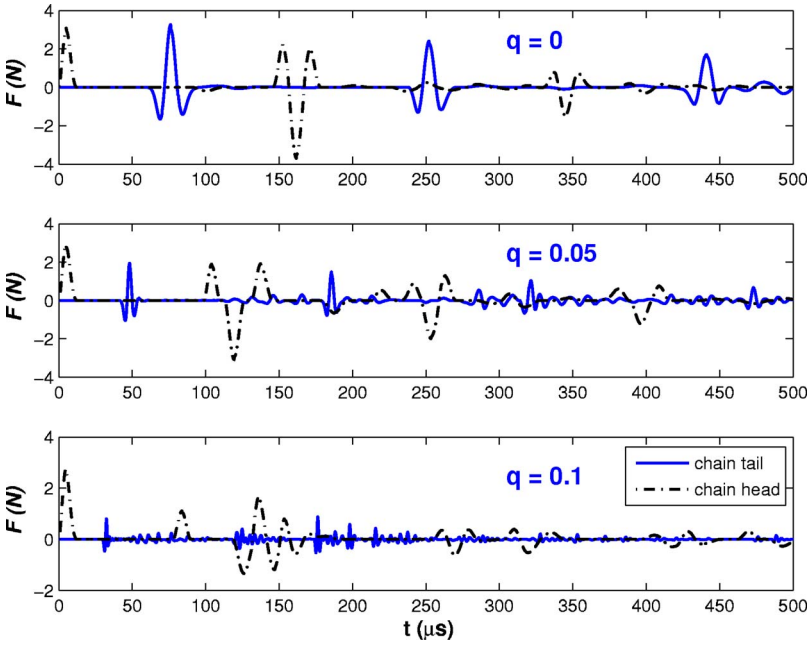

FIG. 5. (Color online) Each of the plots depict force as a function of time for the tail and head particles in a chain with $N=15, \omega=0.05$. The value of the tapering increases for successive plots and is denoted by the label q. Negative forces imply acceleration towards the smaller end of the chain. These plots demonstrate that increased tapering reduces the force felt by the last grain.

[panels (d)–(f)] of Fig. 4 corresponds to a chain with a tapering of 10% so that particles 11–15 have radii 1.74, 1.57, 1.41, 1.27, and 1.14 mm, respectively. Negative velocities and displacement imply motion towards the end of the chain.

For the monodisperse chain, the last five particles first receive and reflect the propagating impulse between 40 and 120 μs. It also appears that for the monodisperse chain, there is about 5 μs of compression for a given grain before it noticeably responds to the contact force and accelerates away. Observe particle 11 acting upon particle 12 in panel (b) of Fig. 4, for example. Additionally, note that after another 5 μs—when particle 11 hits its peak velocity—particle 13 starts to respond to the impulse.

When looking at the peak kinetic energy of particle 13 occurring at 62.5 μs in panels (a)–(c), energy is primarily shared among its two nearest neighbors such that most of the kinetic energy of the system is shared among three adjacent particles. The actual number, within the precision of our calculations, is 5 (to a lesser extent there is a measurable amount of energy in the next layer of nearest neighbors). This is true for any interior particle and is in agreement with Manciu *et al.* [38,39]. These solitary waves [40]—the "envelope" of the five grains in question—represent localized energy that propagates while maintaining its width and suffer a decrease in amplitude during propagation due to restituive losses. The decrease of the tail particle's velocity is a result of the modified potential in Eq. (1) since the boundary is a particle of infinite radius, $R_{i+1} \to \infty$.

At approximately 77 μs, nearly all the energy is briefly stored as elastic potential energy. Simultaneously, particles 14 and 15 are maximally displaced from their equilibrium position while particles 11–13 are still slowly compressing towards the boundary. A close examination about this time shows that the 14th grain is actually the first particle to reverse direction. An exaggerated viewing of the velocities (not shown) reveal that most particles are very slowly moving away from the tail end. This reduced resistance to motion is why the grain velocity increases as one moves back towards the front of the chain [see Fig. 4(b)].

For the highly tapered chain ($q=0.1$) of Figs. 4(d)–4(f), the last five particles first receive and reflect the propagating impulse faster than that of the monodisperse case. As particles 11–14 are accelerated towards the end, their maximum speed increases due to their smaller mass.

What stands out dramatically is the complicated multicollision process of the relative displacements in Fig. 4(d). Keep in mind that particle 15 will be moving the fastest and particle 11 the slowest (of those shown). After the collision with the boundary, the particles begin their rebound with the smallest grains overtaking their larger neighbors. A rapid succession of collisions occur with the distance between centers growing as the group of particles slowly move back to their equilibrium positions, as panel (d) indicates.

When one records the force (Fig. 5) or energy (Figs. 2 and 3) at the end of the tapered chain with a sensor of some sort, the patterns recorded vary for N and q as these plots suggest. As the tapering increases, the pattern changes from a well-defined and periodic pulse to noise. This trend is visible for increasing q in Figs. 2–5 and represents the thermalization that we are looking to exploit in various applications.

B. T_N and F_N parameter space behavior

We evaluate the effectiveness of TCs in decimating impulses based on normalized T and force phase diagrams from parametric studies of N, q, and ω. Such phase diagrams are likely to be useful to the experimentalist [42]. Specifically, we form the ratio $T_N=T_{out}/T_{in}$, where T_{out} is the first peak felt by the last grain and T_{in} is unchanged for chains of the same material. Analogously, F_{out} is the first *minimum* felt by the last grain since the direction of a negative force is into the wall or force sensor. The algorithm to pick out the first turning point for each of these is straightforward. Since $T(t)$ is a column vector, one can iterate through each element until

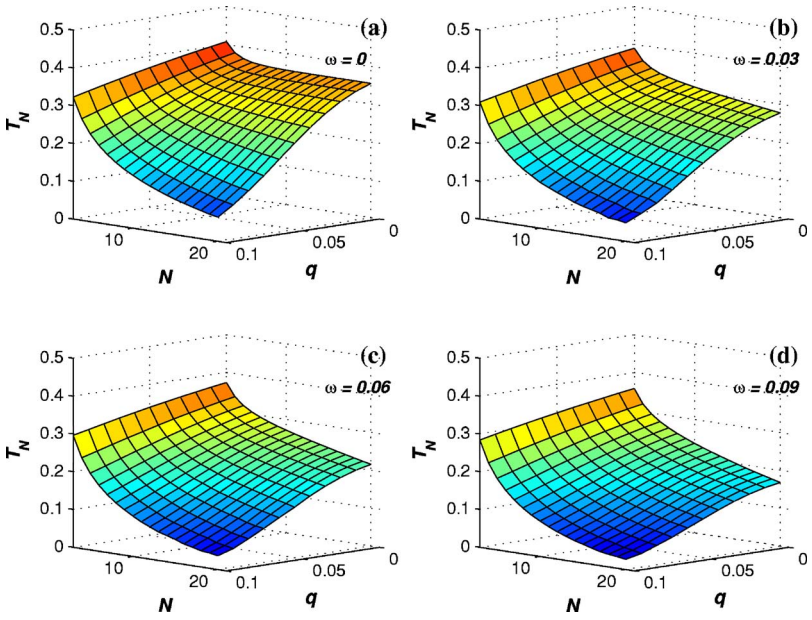

FIG. 6. (Color online) Numerical solution of $T_N(N,q)=T_{out}/T_{in}$ parameter space for constant ω. Observe that energy absorption increases with any combination of N, q, and ω. Additionally, results are independent of system size.

the first occurrence of $(i+1)<i$ is true. In that case, i represents the peak. For force we compare against $(i+1)>i$. Actually, normalization is a critical component in determining the effectiveness of TCs and has been given a more thorough discussion in the Appendix. We have carried out extensive analyses of energy and force absorption exhibited by TCs with various attributes. These studies are summarized via the panels in Fig. 6.

Figure 6 highlights the numerical results for $T(N,q)$ for various values of ω. We find that T decays as a Gaussian function in q and as an exponential function in N. As we shall see later, these dependences can be also found from a simple hard-sphere analysis of these systems.

In the absence of restitution [panel (a)], for $q>0$, the impulse energy is eventually distributed among the other grains as kinetic and potential energies. For monodisperse chains ($q=0$), and N sufficiently small, the solitary wave may not necessarily have a chance to form. Under such circumstances, most of the energy is transmitted as kinetic energy. This is the reason why T_N decreases for increasing N. As discussed earlier, a solitary wave carries approximately 56.5% of its energy as kinetic energy and the rest as potential energy. Hence, as expected, $T(N,q=0,\omega=0)\rightarrow$const. This constant is approximately 0.35 of the input kinetic energy. The reason for why this constant is 0.35 rather than 0.565 is not well understood. However, other studies [37] show that the energy distribution is affected by the presence of end walls. Our findings are consistent with observations by Sen *et al.* [37] and by Pfannes [41]. The results obtained for the monodisperse case serves to check the accuracy of our calculations. For monodisperse chains, as restitution is raised to higher values [see Figs. 6(b)–6(f)], one finds that T_N seems to acquire an exponential-like decay in N. This is evident in Fig. 10. As we shall see, this behavior is consistent with hard-sphere based analysis.

For small chains there are fewer collisions, so restitutive losses do not play a very big role. The same is true for the amount of tapering. If we hold q fixed at a small value and increase N, the chain is *almost* monodisperse. The mismatches are not significant enough and the solitary wave propagation picture remains roughly valid as can be seen by looking at the behavior of T_N for small values of q in Figs. 6(b)–6(d). However, T_N begins to decay dramatically as q is raised beyond 0.05 and N is larger than 10. Besides studying how T_N decays as functions of N, q, and ω, it is important also to study the behavior of the force felt at the tapered end. Such forces can be recorded rather readily using pressure sensors and indeed experimental analyses along those lines have been reported by Nakagawa *et al.* [42]. We consider a discussion of the nature of the force at the tapered end below.

The normalized force for various tapered chains is shown in the panels in Fig. 7. As in the case of T decay with increasing N, the decay of F_N as N increases can be fitted by a one or two phase exponential. The Gaussian decay of F_N as a function of q is less obvious and can be approximated by a plane for $N\gtrsim 5$ throughout the parameter space. In general, the magnitude of F_N appears to be twice that of T_N. The data shown in Fig. 7 suggest that $\sim$ 80% of the input force can be absorbed by a TC with $N=20$, $q=0.10$, and $\omega=0.04$, which are experimentally realizable numbers. Indeed, data obtained by Nakagawa *et al.* [42] using chrome spheres are consistent with what we find.

Below we discuss studies of shock absorption by TCs in the hard-sphere approximation both when there is no energy loss at the granular contacts and when there is. In the absence of a soft potential, it is not possible to construct force phase diagrams. We hence focus only on system energetics. The hard-sphere approximation can be bent around to give a reasonable description of the $T(N,q,\omega\rightarrow E_L)$ that is seen via the extensive dynamical studies.

III. HARD-SPHERE APPROXIMATION

A. Lossless hard-sphere approximation

Ignoring energy losses, we can perform a hard-sphere approximation for a tapered chain which is congruent to the

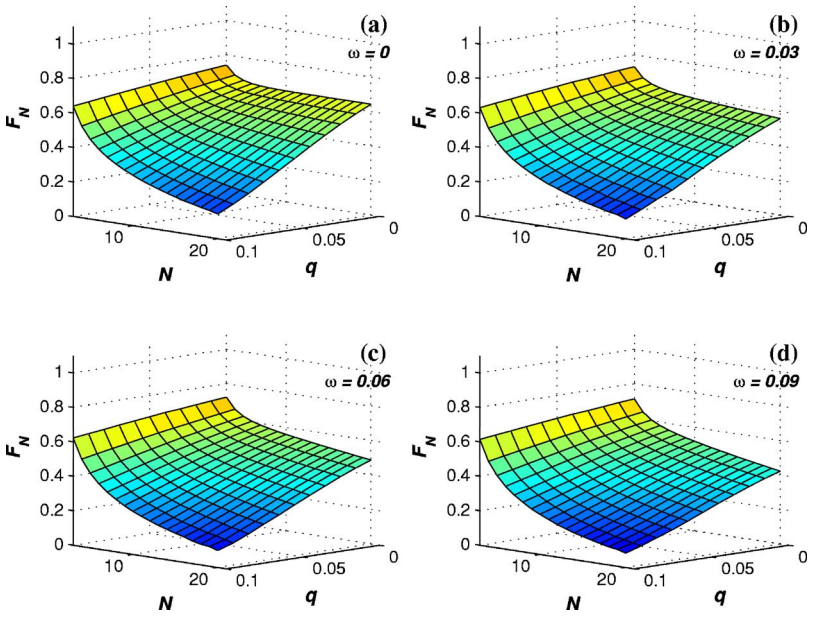

FIG. 7. (Color online) Numerical solution of $F_N(N,q)=F_{out}/F_{in}$ parameter space for constant ω. These plots are similar to those in Fig. 6. For large q, about twice as much energy is absorbed as force.

independent collision model proposed by Wu [32]. By generating an iterative form of the conservation equations, one can arrive at an expression for the normalized kinetic energy, $T_N=T_{out}/T_{in}$. The radius of the $(i+1)$ particle is reduced by $q\%$ from particle i. Therefore masses and radii are expressed as

$$r_{i+1} = r_i - r_i q = (1-q)r_i = \epsilon r_i,$$

$$m_i = \rho V_i = \frac{4}{3}\pi r_i^3 \rho = \eta r_i^3, \tag{6}$$

$$m_{i+1} = \eta r_{i+1}^3 = \eta \epsilon^3 r_i^3, \tag{7}$$

where $\epsilon=1-q$. Evaluating the conservation of momentum with a single prime denoting postcollision values and the initial condition that the $(i+1)$ particle is stationary before a collision $(v_{i+1}=0)$, all η cancel and we obtain

$$m_i v_i + m_{i+1} v_{i+1} = m_i v_i' + m_{i+1} v_{i+1}',$$

$$r_i^3 v_i = r_i^3 v_i' + \epsilon^3 r_i^3 v_{i+1}',$$

$$v_i = v_i' + \epsilon^3 v_{i+1}', \tag{8}$$

where Eqs. (6) and (7) have been used. Following the same procedure for the conservation of energy while ignoring the factor of one-half yields

$$v_i^2 = v_i'^2 + \epsilon^3 v_{i+1}'^2. \tag{9}$$

Letting $A=\epsilon^3 v_{i+1}'$ we can rewrite Eq. (8) in terms of v_i' and substitute the resulting expression into Eq. (9),

$$v_i^2 = (v_i - A)^2 + A v_{i+1}' = v_i^2 - 2A v_i + A^2 + A v_{i+1}',$$

$$2v_i = A + v_{i+1}',$$

$$\frac{v_{i+1}'}{v_i} = \frac{2}{1+\epsilon^3}. \tag{10}$$

Note that for one collision

$$\therefore \frac{T_{out}}{T_{in}} = \frac{T_{i+1}'}{T_i} = \frac{m_{i+1}}{m_i}\left(\frac{v_{i+1}'}{v_i}\right)^2 = \epsilon^3\left(\frac{v_{i+1}'}{v_i}\right)^2$$

$$\therefore \frac{T_{i+1}'}{T_i} = \frac{4\epsilon^3}{(1+\epsilon^3)^2}. \tag{11}$$

For N particles there will be $N-1$ collisions, each of which have the ratio in Eq. (11). Therefore the normalized kinetic energy T_N for the lossless STC hard-sphere approximation is given as

$$T_N = \left\{\frac{4(1-q)^3}{[1+(1-q)^3]^2}\right\}^{N-1}. \tag{12}$$

B. Lossy hard-sphere approximation

The same approximation can be performed with energy losses $\tilde{E}_L$ included such that the system is still conservative. Equation (8) is unchanged, but Eq. (9) becomes

$$v_i^2 = v_i'^2 + \epsilon^3 v_{i+1}'^2 + \tilde{E}_L. \tag{13}$$

One then obtains a more complicated expression replacing Eq. (10),

$$\frac{v_{i+1}'}{v_i} = \frac{2 - \dfrac{\tilde{E}_L}{\epsilon^3 v_i v_{i+1}'}}{1+\epsilon^3}. \tag{14}$$

We can make the substitution $\tilde{E}_L \propto v_i v_{i+1}'$ or $\tilde{E}_L = E_L v_i v_{i+1}'$ where E_L is the constant of proportionality. Rearranging Eq. (14) after the simplification yields

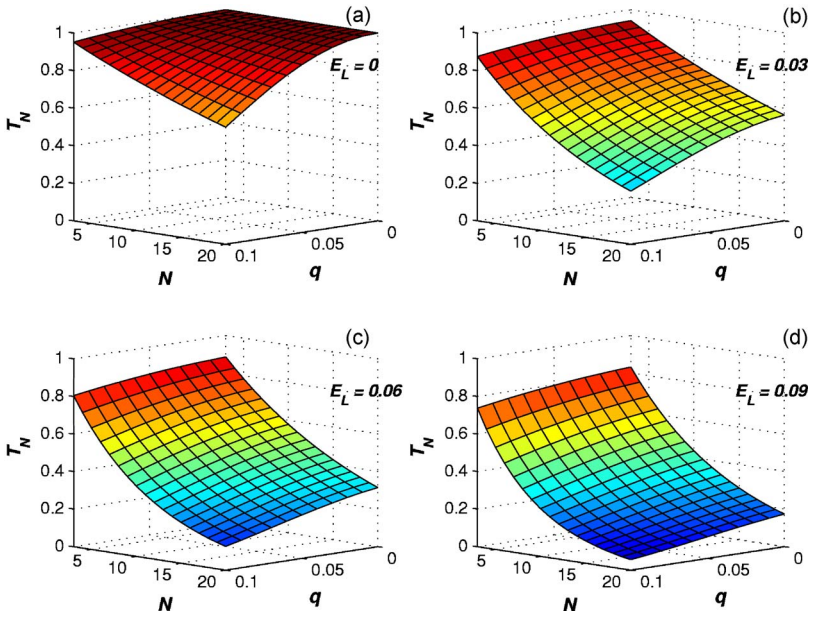

FIG. 8. (Color online) $T_N(N,q,E_L)$ parameter space for the TC in the hard-sphere approximation. N varies from 3 to 25 and q from 0–20 %.

$$\frac{v'_{i+1}}{v_i} = \frac{2\epsilon^3 - E_L}{\epsilon^3(1+\epsilon^3)}.$$

The corresponding result for the normalized kinetic energy for N particles is

$$T_N = \left\{ \frac{[2(1-q)^3 - E_L]^2}{(1-q)^3[1+(1-q)^3]^2} \right\}^{N-1}. \tag{15}$$

Note that in the limit $E_L=0$, Eq. (15) reduces to the lossless case in Eq. (12) as expected. Also, results are independent of initial velocity and size of the grains. The latter suggests an inherent scale invariance to these systems. All energy in the hard-sphere approximation is manifested as kinetic and the width of the energy bundle is one sphere.

C. Kinetic energy parameter space for hard-sphere TCs

Figure 8 shows the behavior described by Eq. (15) for $0 \leqslant q \leqslant 0.1, 3 \leqslant N \leqslant 20$, and for selected values of the energy loss parameter E_L. It may be observed that for $q=E_L=0$ and any N, the T plotted along the vertical axis of Fig. 8(a) is unity as expected. For these lossless monodisperse chains, kinetic energy is completely transferred from one end of the chain to the other regardless of the number of spheres involved. In earlier work, this simple limit has been identified with the problem of solitary wave propagation through a chain of Hertz spheres [see Eq. (1)] where the Hertz law becomes infinitely repulsive, i.e., $V(\delta_{i,i+1}) \sim \delta_{i,i+1}^n$, where $n \to \infty$.

Our studies reveal that the T_N decays as a Gaussian function in tapering q (when the axes are extended—see Fig. 9). For small systems, that is when N is small enough, one observes a linear decay of T as function of q. This behavior can be gleaned from Eqs. (12) and (15). We find that T_N decays as an approximately exponential function in N. As we shall see, these properties of $T(n,q)$ are also present in the full scale dynamical studies where the Hertz potential between the spheres is taken into account.

If the initial velocity is supplied to the smaller end of the tapered chain, one also observes shock absorption similar to the system in Fig. 1: albeit with less efficiency. The main reason as to why an "inverse" TC is a shock absorber is due to the fact that a small mass cannot transfer significant amounts of energy to a larger mass and hence much of the energy remains trapped at the tapered end. The analytic calculations needed to construct a phase diagram for the inverse TC is accomplished by adjusting the definition of tapering. In this case, subsequent particles are growing in size, i.e., $r_{i+1}=(1+q)r_i$. Equations (12) and (15) are modified accordingly, and the behavior of T_N as functions of q and N for a lossless system is shown in Fig. 9.

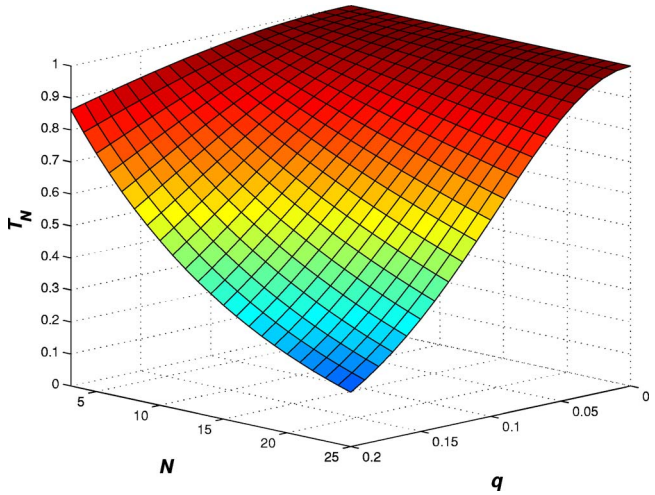

FIG. 9. (Color online) $T_N(N,q)$ parameter space for the TC hard-sphere approximation where initial velocity is supplied to the smaller end of the chain (reference Fig. 1). These results with those of Fig. 8 suggest that adjacent, antiparallel arrangements of tapered chains could work in tandem to mitigate blast effects.

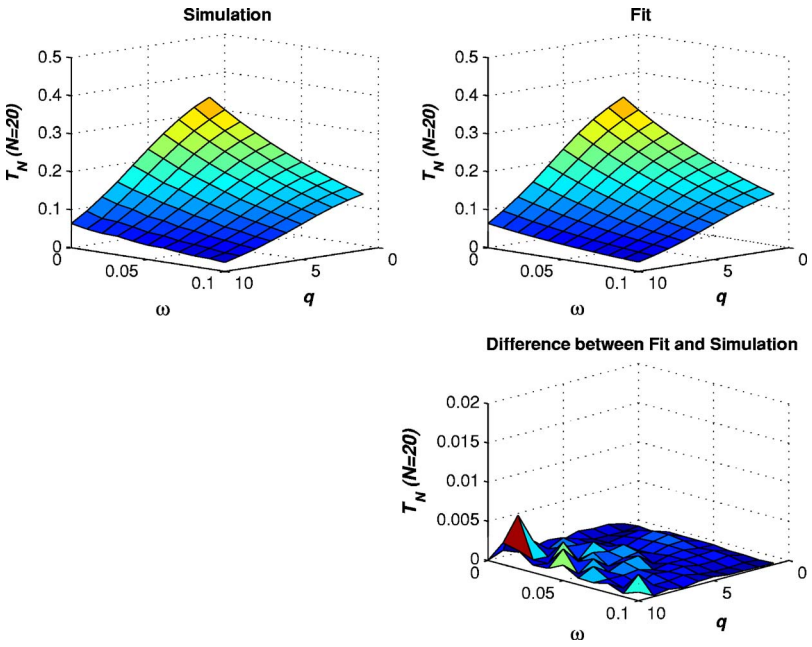

FIG. 10. (Color online) The simulated simple tapered chain and functional fit. Ripples in the simulation for large q are caused by a time step that is not small enough. Differences between the simulation and fit are negligible.

The numerical results can be compared to a scaled hard-sphere approximation and by plotting their difference (not shown). Differences in the two arise from compressive effects or collisions which become more important (frequent) with increasing q and N.

IV. FUNCTIONAL FIT

We propose a functional fit for the $T_N = T_N(\omega, q, N \gtrsim 10)$ parameter space of the form

$$T_N(\omega, q) = A e^{Bq^C} e^{D\omega^E}, \tag{16}$$

which corresponds to a two-dimensional Weibull distribution. Due to the Gaussian and exponential natures of q and ω, respectively, the form in Eq. (16) then is well suited when the exponents are restricted to $C > 1$ and $E \leqslant 1$. For simplicity we set $E=1$ and $C=3/2$. The coefficients B and D were evaluated using fourth-order polynomial fits and the scaling coefficient A is essentially the point $T_N(N, \omega = q = 0)$. It turns out that a second-order fit was not sufficiently robust and a higher-order fit yielded marginal gains at the cost of mathematical encumbrance. Note that this fit is for $T_N(q, \omega, \text{const } N)$ whereas kinetic energy parameter space plots in this report have been of the form $T_N(q, N, \text{const } \omega)$.

This fit currently lacks the rigor sufficient for planar behavior in the limit of small N. It is unclear at this point if N can be completely decoupled from ω and q and written as an additional exponential term. In all likelihood, the coefficients B and D would be written as functions of N. Ultimately, it would be useful to expand Eq. (16) which describes the normalized kinetic energy as a function of N, q, ω, and F_{load} where the latter is an external loading or precompression of the chain.

In evaluating the fits, we find that $T_N(\omega, q, N=20)$ is described quite well by

$$\begin{aligned} T_N(\omega, q) = {} & 0.355\,44 \\ & \times \exp([-1.5055 \times 10^{-5} q^4 + 4.016 \times 10^{-4} q^3 \\ & - 3.981 \times 10^{-3} q^2 + 0.0147 q - 0.054\,35] q^{3/2}) \\ & \times \exp([4.144 \times 10^{-5} q^4 + 1.955 \times 10^{-3} q^3 \\ & - 0.039\,62 q^2 + 0.028\,87 q - 8.341] \omega). \end{aligned} \tag{17}$$

Figure 10 compares the numerical results and the fit for the case of $N=20$. The results are practically indistinguishable except for the minor time-step errors in the simulation which lead to the roughness in the difference plot for large q. For this large value of N and q, the tail particle is rather small and has a large velocity. The time step is such that kinetic energy plots lose their accuracy because the algorithm picking the first peak is seeing less smoothness in the $T(t)$ arrays. As such, the fit provides a better assessment for the state of the system.

V. SUMMARY AND CONCLUSION

In this work, we have focused on small TCs with N numbering between 3 and 20 grains and with tapering and restitution spanning 0–10 %. To our knowledge, the chosen parameter space captures the energy absorption characteristics of most TCs that can be realized in laboratory settings. Our focus has been on carrying out grain level dynamical analyses and on the construction of phase diagrams to characterize force and energy absorption.

We have reported an exhaustive investigation of how the kinetic energy of an impulse is converted to kinetic and potential energies in grains of monodisperse and tapered chain systems. Our analyses describe the behavior of kinetic energy of the smallest grain at the tapered end to that of the largest grain—where we assume the impulse is incident—as functions of number of grains, tapering, and restitution. Similar studies have also been done for the force felt by the

smallest grain. The phase diagrams are found to have an intriguing form that can be captured for fixed number of grains as a two-dimensional Weibull distribution. We have next reconstructed the phase diagrams using a simple hard-sphere based analysis. When there is no dissipation, we have recovered the results reported earlier by Wu [32]. We subsequently introduced dissipation within the framework of a hard-sphere model. The phase diagrams were constructed to describe how kinetic energy of the last grain depends upon the number of grains, the tapering, and the restitution. Apart from a normalization constant that needs to be introduced to make a correction for neglecting potential energy (which must be done in a hard-sphere based study) we are able to describe most of the effects found in the full scale dynamical analyses. However, the hard-sphere approximation is not useful for constructing force phase diagrams, ones that could be more useful to the experimentalists.

Finally, we extend our hard-sphere analysis to probe tapered chains where the impulse is incident at the tapered end and find that such an "inverse" tapered chain also is a good shock absorber. Thus space filling combinations of tapered chains and inverse tapered chains may be useful in the construction of shock absorbing systems.

ACKNOWLEDGMENTS

Much appreciation goes to the U.S. Army Research Laboratory (ARL) for their continuing financial support of one of us (R.L.D.). We would also like to acknowledge Brian Leavy, Dr. John Powell, Dr. Carl Krauthauser, Dr. Mike Normandia, Dr. Bob Frye, Brian Powell, Dr. Gerald Jullien, Professors Francisco Melo, Stephane Job, Masami Nakagawa, and Dr. Juan Agui, Jr. for their interest in this work. We acknowledge many discussions with Adam Sokolow and Jan M. M. Pfannes during the course of this work. S.S. has been supported by NSF during the course of much of the research reported here.

APPENDIX: NORMALIZATION

Normalization has posed some challenges in trying to properly assess the absorption quality of a TC. Recall that the goal is to measure the energy at the last grain versus the energy put into the system via an input velocity to the first. In general, adjustments to the normalization scheme will simply scale the kinetic energy parameter space surface. In some cases [41], the output value of each chain is based on the maximum possible force felt by any possible chain under consideration (i.e., monodisperse and no energy loss). This gives a measure of how one chain is better than another. In this communication, we have chosen to form the ratio based on the outputs felt by each specific chain. This serves to grade the individual effectiveness of any chain without reference to another.

In choosing a peak value with this method, one could identify either when the impulse first hits the last grain or look for the maximum peak whenever it may occur. We have chosen to use the former for several reasons. First it ignores the complexity of nonlinear reverberations which, especially in the case of zero restitution, can lead to large peaks at unpredictable times. Second, we argue that for systems with finite restitution, the possibility of observing a large peak at late times is practically absent due to attenuation effects.

There are special cases, however, where the maximum may occur at later times which needs to be investigated further. In Fig. 3 for $q=0.1$ for example, we see the obvious spike at about 225 μs which is much stronger than the initial arrival at 35 μs. This is one of those instances that disagree with our normalization method; however, it is an exception rather than the rule. We have investigated this particular case further without including extraneous plots and report the following observations. The effect exists for $N=15$–20 for $\omega \leqslant 0.03$. When $N=20$ is held fixed and restitution is further increased, the peak kinetic energy once again occurs for the first arrival of the pulse. As q increases, so do the number of collisions and the requisite energy loss through them. For small N, however, the peak can be anywhere. A possible dynamical reason for such simplification may be due to collective motion of most grains towards the end wall, which at certain points in time can dramatically increase the velocity of the smallest grain.

Under a normalization with the maximum output peak occurring at any time, the force surfaces can yield $F_{out}/F_{in} \geqslant 1$. Such force amplification is not completely unexpected as it is seen in (nonlinear) rods [43] and the latter has been shown to be mathematically similar to granular media [44]. Therefore for longer chains, it is more typical to encounter the global peak when the impulse first reaches the tail particle.

[1] J. Duran, *Sands, Powders, and Grains* (Springer, Berlin, 2000).
[2] *Granular Matter*, edited by A. Mehta (Springer, Berlin, 1994).
[3] J. Kakalios, Am. J. Phys. **73**, 8 (2005).
[4] H. P. Rossmanith and A. Shukla, Acta Mech. **42**, 211 (1982).
[5] H. M. Jaeger and R. Nagel, Science **255**, 1523 (1992).
[6] H. M. Jaeger, R. Nagel, and R. P. Behringer, Rev. Mod. Phys. **68**, 1259 (1996).
[7] V. F. Nesterenko, J. Appl. Mech. Tech. Phys. **5**, 733 (1983).
[8] A. N. Lazaridi and V. F. Nesterenko, J. Appl. Mech. Tech. Phys. **26**, 405 (1985).
[9] V. F. Nesterenko, J. Phys. IV **55**, C8 (1994).
[10] V. F. Nesterenko, A. N. Lazaridi, and E. B. Sibiryakov, J. Appl. Mech. Tech. Phys. **36**, 166 (1995).
[11] R. S. Sinkovits and S. Sen, Phys. Rev. Lett. **74**, 2686 (1995).
[12] S. Sen and R. S. Sinkovits, Phys. Rev. E **54**, 6857 (1996).
[13] C. Coste, E. Falcon, and S. Fauve, Phys. Rev. E **56**, 6104 (1997).
[14] S. Sen and M. Manciu, Phys. Rev. E **64**, 056605 (2001).
[15] M. Manciu, S. Sen, and A. J. Hurd, Physica D **157**, 226

(2001).
[16] S. Sen, F. S. Manciu, and M. Manciu, Physica A **299**, 551 (2001).
[17] S. Job, F. Melo, A. Sokolow, and S. Sen, Phys. Rev. Lett. **94**, 178002 (2005).
[18] H. Hertz, J. Reine Angew. Math. **92**, 156 (1882).
[19] L. D. Landau and E. M. Lifshitz, *Theory of Elasticity* (Pergamon, Oxford, 1970), p. 30.
[20] A. E. H. Love, *A Treatise on the Mathematical Theory of Elasticity* (Dover, New York, 1955).
[21] B. Leroy, Am. J. Phys. **53**, 346 (1985).
[22] V. F. Nesterenko, *Dynamics of Heterogeneous Materials* (Springer, New York, 2001).
[23] D. F. Strenzwilk, J. Appl. Phys. **50**, 6767 (1979).
[24] J. Tasi, J. Appl. Phys. **43**, 4016 (1972); **44**, 4569 (1973); **51**, 5804 (1980); **51**, 5816 (1980).
[25] J. Batteh and J. Powell, J. Appl. Phys. **49**, 3933 (1978).
[26] J. H. Batteh and J. D. Powell, Phys. Rev. B **20**, 1398 (1979).
[27] J. Powell and J. Batteh, J. Appl. Phys. **51**, 2050 (1980).
[28] N. J. Zabusky and M. D. Kruskal, Phys. Rev. Lett. **15**, 240 (1965).
[29] D. J. Korteweg and and G. de Vries, Philos. Mag. **39**, 422 (1895).
[30] E. Fermi, J. Pasta, and S. Ulam, *The Collected Works of Enrico Fermi*, "Studies of Non Linear Problems" (University of Chicago Press, Chicago, 1965), Vol. 2. p. 978. Also in Los Alamos Report, Document No. LA-1940.
[31] M. Toda, *Theory of Nonlinear Lattices* (Springer, New York, 1978).
[32] D. T. Wu, Physica A **315**, 194 (2002).
[33] O. R. Walton and R. L. Braun, J. Rheol. **30**, 949 (1986).
[34] W. J. Stronge, *Impact Mechanics* (Cambridge, Cambridge, England, 2000).
[35] http://www.matweb.com/
[36] M. P. Allen and D. J. Tildesley, *Computer Simulation of Liquids* (Clarendon, Oxford, 1987).
[37] A. Sokolow, J. M. M. Pfannes, R. L. Doney, M. Nakagawa, J. Agui, and S. Sen (unpublished).
[38] M. Manciu, S. Sen, and A. J. Hurd, Physica A **274**, 588 (1999).
[39] M. Manciu, S. Sen, and A. J. Hurd, Physica A **274**, 607 (1999).
[40] M. Remoissenet, *Waves Called Solitons* (Springer, Berlin, 1999), 3rd ed.
[41] J. Pfannes, M.S. thesis, SUNY, Buffalo, 2003.
[42] M. Nakagawa, J. Agui, D. T. Wu, and D. V. Extramiana, Granular Matter **4**, 167 (2003).
[43] M. Normandia (private communication).
[44] T. Wright, Ballistics Research Lab Technical Report No. BRL-TR-02584, 1984.